

1 **Coral Mortality Event in the Flower Garden Banks of the Gulf of**
2 **Mexico in July 2016: Local Hypoxia due to Cross-Shelf Transport**
3 **of Coastal Flood Waters?**

4
5 Matthieu Le Hénaff^{1,2}

6 Frank E. Muller-Karger³

7 Vassiliki H. Kourafalou⁴

8 Daniel Otis³

9 Kimberley A. Johnson⁵

10 Lucas McEachron⁶

11 HeeSook Kang⁴

12
13 ¹University of Miami/Cooperative Institute for Marine and Atmospheric Studies (CIMAS),

14 4600 Rickenbacker Causeway, Miami, FL 33149-1098, USA

15 ²NOAA Atlantic Oceanographic and Meteorological Laboratory (AOML), 4301

16 Rickenbacker Causeway, Miami, FL 33149, USA

17 ³University of South Florida, College of Marine Science (USF CMS), 140 7th Avenue South,

18 St. Petersburg, FL 33701, USA

19 ⁴University of Miami/Rosenstiel School of Marine and Atmospheric Science (RSMAS), 4600

20 Rickenbacker Causeway, Miami, FL 33149-1098, USA

21 ⁵NOAA Southeast Fisheries Science Center (SEFSC), 75 Virginia Beach Dr, Miami, FL

22 33149, USA

23 ⁶Florida Fish and Wildlife Conservation Commission (FWC), 100 8th Ave SE, St. Petersburg,

24 FL 33701, USA

25

26

Corresponding author:

27

Matthieu Le Hénaff

28

UM/CIMAS, NOAA Atlantic Oceanographic and Meteorological Laboratory (AOML)

29

4301 Rickenbacker Causeway, Miami, FL 33149, USA

30

Tel: (1) 305 361 4435

31

m.lehenaff@miami.edu

32

33 **Abstract**

34 Remotely sensed and *in situ* data, in tandem with numerical modeling, are used to
35 explore the causes of an episode of localized but severe mortality of corals, sponges, and other
36 invertebrates at the Flower Garden Banks (FGB) National Marine Sanctuary in July 2016. At
37 about 190 km off the Texas coast, at the top the seamount in the East FGB, up to 82% of coral
38 reef organisms were affected in a 1 to 2 m thick layer on the local seafloor at ~23 m depth.
39 Analysis of available data pointed to low levels of dissolved oxygen being the most likely
40 contributing factor in the observed mortality (Johnston et al., 2019).

41 Observations show that upwelling-favorable winds in June and July 2016 carried
42 brackish and turbid coastal waters across the northwestern Gulf of Mexico continental shelf to
43 the FGB. This plume of coastal water was the result of exceptionally high precipitation and
44 local river run-off. Field data provide clear evidence of thin, localized, subsurface near-hypoxic
45 layers immediately below this turbid, low salinity coastal plume. These mid-water layers
46 extended over longer distances (30 to 40 km), and reached further offshore (~100 km), than
47 previously reported in the region, associated with large quantities of organic matter carried
48 offshore by the brackish plume.

49 The surface brackish layer was observed to cover the East FGB in satellite ocean color
50 imagery and *in situ* salinity measurements in late June and July 2016. Model results and sparse
51 observations on the shelf suggest that this surface layer was ~20 m thick. It is expected that
52 organic matter carried in the surface layer accumulated on the seafloor of the East FGB, which
53 was just below the brackish plume. In the absence of ventilation, this led to the local formation
54 of a bottom hypoxic layer, similar to what is observed on the Gulf of Mexico inner to mid-shelf
55 every summer.

56 The conditions experienced at FGB in July 2016 are likely to affect other reefs exposed
57 to brackish plumes with high organic matter loads. The processes of physical connectivity by
58 transport of material is critical for reef colonization and survival, but can also be fatal to coral
59 ecosystems. The monitoring of coral reefs should take the threat of hypoxia due to distant
60 sources of organic matter into account.

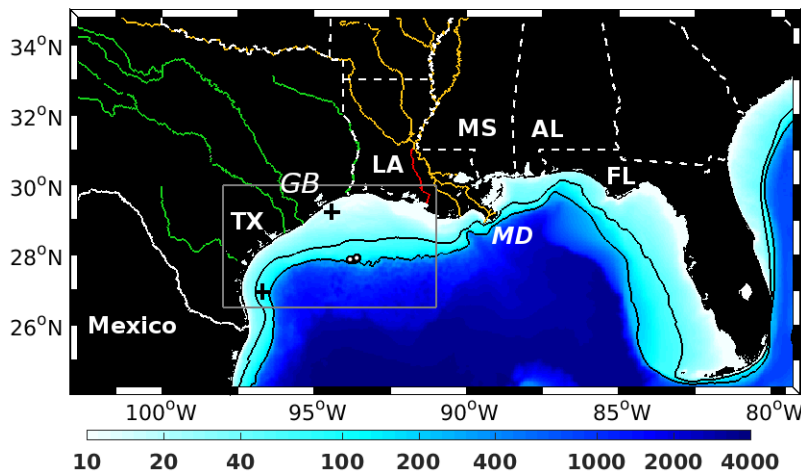
61

62 **Keywords:** Hypoxia; Coral Reef; Upwelling; Shelf Processes; Coastal Flooding; Connectivity;
63 Ecology.

64

65 **1. Introduction**

66 The Flower Garden Banks (FGB) National Marine Sanctuary is located at the Louisiana-
67 Texas (LATEX) shelf break in the northwestern Gulf of Mexico (GoM), between about 110
68 and 190 km offshore (Figure 1). It includes three separate sites, namely the East FGB, West
69 FGB, and Stetson Bank. These small seamounts feature high biodiversity coral reef ecosystems,
70 at depths ranging from ~17 m to ~130 m for the East FGB site (Spalding and Bunting, 2004;
71 Hickerson et al., 2008; Schmahl et al., 2008; Johnston et al., 2019).



72
73 *Figure 1: Bathymetry (m) of the northern Gulf of Mexico (GoM). The white circles with*
74 *black outlines indicate the locations of the East and West Flower Garden Bank seamounts. The*
75 *rivers merging to form the Mississippi River are indicated in orange, while the Atchafalaya*
76 *River is indicated in red. The rivers flowing in the northwestern GoM west of the Mississippi*
77 *and Atchafalaya Rivers are indicated in green. The border between the U.S. and Mexico is*
78 *indicated with a solid white line. The borders between the U.S. states are indicated with dashed*
79 *white lines. States boarding the GoM are labeled as: Texas (TX), Louisiana (LA), Mississippi*
80 *(MS), Alabama (AL), and Florida (FL). The Mississippi Delta and Galveston Bay are marked*
81 *with MD and GB, respectively. The black contours represent the isobaths at 50 and 200 m. The*
82 *black crosses near the coast indicate the locations of the meteorological NOAA NDBC buoys:*

83 42020 (26.97°N; 96.67°W) close to the U.S.-Mexico border, and 42035 (29.23°N; 94.41°W) off
84 Galveston Bay, Texas. The grey frame outlines the focus region of subsequent figures.

85

86 On July 25, 2016, SCUBA divers conducting a survey of the East FGB reported the
87 presence of hazy waters and dead invertebrates, including corals and sponges. Sanctuary
88 personnel responded immediately and organized an oceanographic survey in and around the
89 Sanctuary in the following days, in order to characterize the mortality event and determine its
90 origin and cause. The diver survey found that an area of approximately 5.6 ha (2.6% of the coral
91 reef) on the seafloor at the top of the East FGB coral ecosystem, at about 23 m depth, was
92 affected with mortality affecting up to 82% of organisms in a 1-2 m thick band; organisms
93 above this thin layer at the seafloor, or at deeper depths, were not affected (Johnston et al.,
94 2019). The cause of the mortality was not identified at the time. Yet the analysis of the water
95 quality parameters, the patterns of mortality on the reefs, and observations of dissolved oxygen
96 concentrations DO sensors <3.5 mg/L at similar depths 50 to 70 km northwest of East FGB,
97 suggests that the most likely cause for death of organisms was low levels of dissolved oxygen,
98 i.e., hypoxia (Johnston et al., 2019).

99 The aspect of the organisms affected by the mortality event was similar to that seen
100 during the hypoxia event reported by Altieri et al. (2017) in the Caribbean coast of Panama
101 (Johnston et al., 2019). Altieri et al. (2017) estimated that over 10% of coral reefs around the
102 world are exposed to elevated risks of hypoxia, and that this threat has probably been
103 underreported. However, coral reefs located hundreds of kilometers away from rivers and
104 continental coastal zones, such as the FGB, are generally considered to be safe from such a
105 threat.

106 Several questions remain about the 2016 FGB mortality event. In particular, what were
107 the regional oceanographic conditions associated with that episode of mortality? What could
108 explain the localized mortality of corals and sponges in a limited depth range at the top of the
109 East FGB, while no similar mortality was observed at the West FGB, only 20 km away? To
110 address these questions, we examined and documented the timeline of physical oceanographic
111 events over the northwestern GoM in the weeks prior to and during the mortality event. Our
112 approach is based on the use of satellite ocean color data, combined with *in situ* measurements
113 and outputs from a realistic model simulation.

114 A wide variety of satellite-based remote sensing techniques have been used to examine
115 the distribution and temporal variability of optical characteristics of surface waters of the GoM.
116 Arnone et al. (2017) used imagery from the Visible Infrared Imaging Radiometer Suite (VIIRS)
117 to examine diurnal changes in phytoplankton biomass in the eastern GoM. Schaeffer et al.
118 (2015) evaluated a suite of algorithms to estimate CDOM absorption in estuaries in the northern
119 GoM and found that a reflectance ratio using red and blue bands provided the best fit between
120 field and satellite data. D'Sa et al. (2007) developed a two-band reflectance algorithm based on
121 red and green bands to estimate suspended particulate matter concentrations in the northern
122 GoM. This band ratio is related to the backscattering coefficient at 555nm. Previous work has
123 demonstrated the utility of ocean color observations to trace physical connectivity patterns in
124 this region (Muller-Karger et al., 1991; Hu and Muller-Karger, 2008; Soto et al., 2009). In this
125 study, we used the Chlorophyll-a product from MODIS and VIIRS to examine temporal
126 patterns of turbid waters that were transported from the coastal GoM to the FGB reefs.

127 The northwestern Gulf of Mexico (NWGoM), where the mortality event took place,
128 encompasses a wide shelf south of Louisiana and Texas, the LATEX shelf. This shelf is narrow
129 in its western portion near the U.S. and Mexico border, wide in its central part (~200 km), and
130 narrow again in the east near the Mississippi Delta. Tidal currents at the shelf break are weak

131 (~3 cm/s), but increase to the north as the shelf gets shallow, reaching about 10 cm/s along the
132 Louisiana coast; they are typically low (~2 cm/s) close to the U.S.-Mexican border (DiMarco
133 and Reid, 1998). The lower frequency circulation over the inner shelf is mostly driven by winds.
134 Winds are easterly (i.e., from the east) for most of the year, but turn to southerly in summer
135 (Nowlin et al., 2005; Zavala-Hidalgo et al., 2014). As a result, the wind-driven circulation over
136 the LATEX shelf is westward most of the year, with more intense currents near the coast. In
137 summer, this circulation reverses to eastward due to changes in wind direction (Nowlin et al.,
138 2005). Changes in the wind pattern in summer also lead to upwelling along the western coast,
139 near the border between the U.S. and Mexico (Zavala-Hidalgo et al., 2006). The LATEX outer
140 shelf waters are subject to frequent interactions with mesoscale eddies, which are common in
141 the deep GoM (e.g. Biggs and Muller-Karger, 1994; Hamilton et al., 2002). A one-year long
142 survey at the East FGB showed strong inertial currents and weak tidal currents, and confirmed
143 the importance of the wind and eddies in driving the circulation in the FGB area (Teague et al.,
144 2013). Although the East and West FGB form small seamounts, typical physical processes
145 associated with the presence of seamounts, such as Taylor Columns, doming of density
146 surfaces, enclosed circulation cells and enhanced vertical mixing (e.g. White et al., 2007), have
147 not been reported at the FGB to our knowledge.

148 The mid- and inner LATEX shelf presents widespread hypoxic to anoxic conditions
149 every summer (Rabalais et al., 2002). This is attributed to the decay of phytoplankton blooms
150 and other organic matter associated in great measure with the discharge from the Mississippi
151 and Atchafalaya Rivers (Dale et al., 2007; Conley et al., 2009; Levin et al., 2009). Bacterial
152 consumption of this material and respiration lead to widespread oxygen depletion, which affects
153 the shelf pelagic and benthic ecosystems, leading to stress and mortality of organisms (Rabalais
154 et al., 2001). The dynamics of the Mississippi/Atchafalaya River plume plays a major role in
155 the intensity of the hypoxia episodes. Typically, easterly winds strengthen the buoyancy-driven

156 westward river plume circulation along the LATEX shelf. Conversely, southerly winds in the
157 summer favor accumulation of brackish waters west of the Mississippi Delta and eastward
158 advection of waters from the Mississippi and other rivers to the east of the Delta, where they
159 are prone to interacting with the deep GoM current system (Walker et al., 1996; Kourafalou et
160 al., 1996; Muller-Karger et al., 1991, 2015; Muller-Karger, 2000; Morey et al., 2003; Schiller
161 et al., 2011; Androulidakis et al., 2015). Local river discharge and stratification have important
162 effects on the vertical structure of the dissolved oxygen concentration (Hetland and DiMarco,
163 2008; Bianchi et al., 2010). Although the Mississippi/Atchafalaya system is considered to be
164 the main source of nutrients leading to hypoxia in the NWGoM, other rivers also contribute to
165 hypoxic conditions on the shelf, such as the Brazos River in Texas (DiMarco et al., 2012).
166 Despite the recurrence of hypoxia in coastal and shelf waters of the northern GoM, no hypoxic
167 conditions had previously been reported for the FGB.

168 The present article is organized as follows: Section 2 describes the data used in our study
169 of the environmental conditions associated with the 2016 mortality event at the East FGB.
170 Section 3 describes the physical conditions and circulation patterns in the NWGoM during June
171 and July 2016, and the vertical structure of the ocean in that region in June 2016, based on
172 observation data. Section 4 provides a discussion of our results, together with our scenario to
173 explain the observed mortality, and presents our conclusions.

174

175 **2. Data: observations and model simulation**

176 We used ocean color satellite imagery to trace the accumulation and dispersal of turbid
177 coastal waters over the LATEX shelf. Maps of Chlorophyll-a concentration (Chl-a) at 1-km
178 resolution were derived from the Moderate Resolution Imaging Spectroradiometers (MODIS)
179 on NASA's Aqua and Terra satellites (2014 reprocessing) and from the Visible Infrared

180 Imaging Radiometer Suite (VIIRS) on NOAA's Suomi satellite. Level-2 daily satellite pass
181 files for the study region were obtained from NASA's Ocean Biology Processing Group
182 (<https://oceancolor.gsfc.nasa.gov/>) and subsequently binned to weekly intervals. Chl-a was
183 estimated using NASA's default chlor_a product (Hu et al., 2012; O'Reilly, 2000). We are
184 aware that, in river-dominated coastal and shelf areas, the Chl-a ocean color has a higher
185 uncertainty due to the various other constituents present in the water, including CDOM (e.g.
186 Muller-Karger et al., 1991; Hu et al., 2003; Nababan et al., 2011). However, satellite Chl-a has
187 a lesser level of noise compared to CDOM estimates, which makes it an appropriate choice for
188 tracing the details of the coastal water displacements (Brown et al., 2008; Otis, 2012; Otis et
189 al., 2019). Since ocean color Chl-a estimates have large errors in turbid coastal waters, the Chl-
190 a values presented in this study are not expected to be an accurate estimate of the actual
191 Chlorophyll-a concentration, and we will refer to these values as 'apparent' Chl-a.

192 Daily satellite-derived Sea Surface Temperature (SST) maps were used to identify
193 coastal upwelling regions where cooler water surfaced near the coast and spread over the shelf.
194 SST maps were extracted from the Multiscale Ultrahigh Resolution (MUR) Sea Surface
195 Temperature dataset from the Group for High Resolution Sea Surface Temperature (GHRSSST).
196 The data (2003-2017) were obtained from NASA at a global 0.011° spatial grid. The product
197 amalgamates SST observations from several instruments, including the NASA Advanced
198 Microwave Scanning Radiometer-EOS (AMSRE) and the Moderate Resolution Imaging
199 Spectroradiometer (MODIS).

200 *In situ* data were used to complement the remotely sensed data. Wind data were obtained
201 from buoys 42020 and 42035 from NOAA's National Data Buoy Center (NDBC). Buoy 42020
202 (26.97°N; 96.67°W) is located close to the U.S.-Mexico border, and buoy 42035 (29.23°N;
203 94.41°W) is off Galveston Bay, Texas (Figure 1). Surface salinity data was obtained from the
204 Texas Automated Buoy System (TABS) database (TABS 2018), at buoys V and N located at

205 East and West Flower Garden Banks, respectively. River discharge data for rivers in the region
206 were obtained from the U. S. Geological Survey (USGS) and the U.S. Army Corps of
207 Engineers. Finally, hydrographic sections over the NWGoM shelf were obtained from the June
208 2016 cruise of the NOAA R/V *Oregon II*. These data included vertical profiles of temperature,
209 salinity, dissolved oxygen concentration, transmissometry (c-beam attenuation coefficient at
210 660 nm), and fluorometry collected during CTD casts.

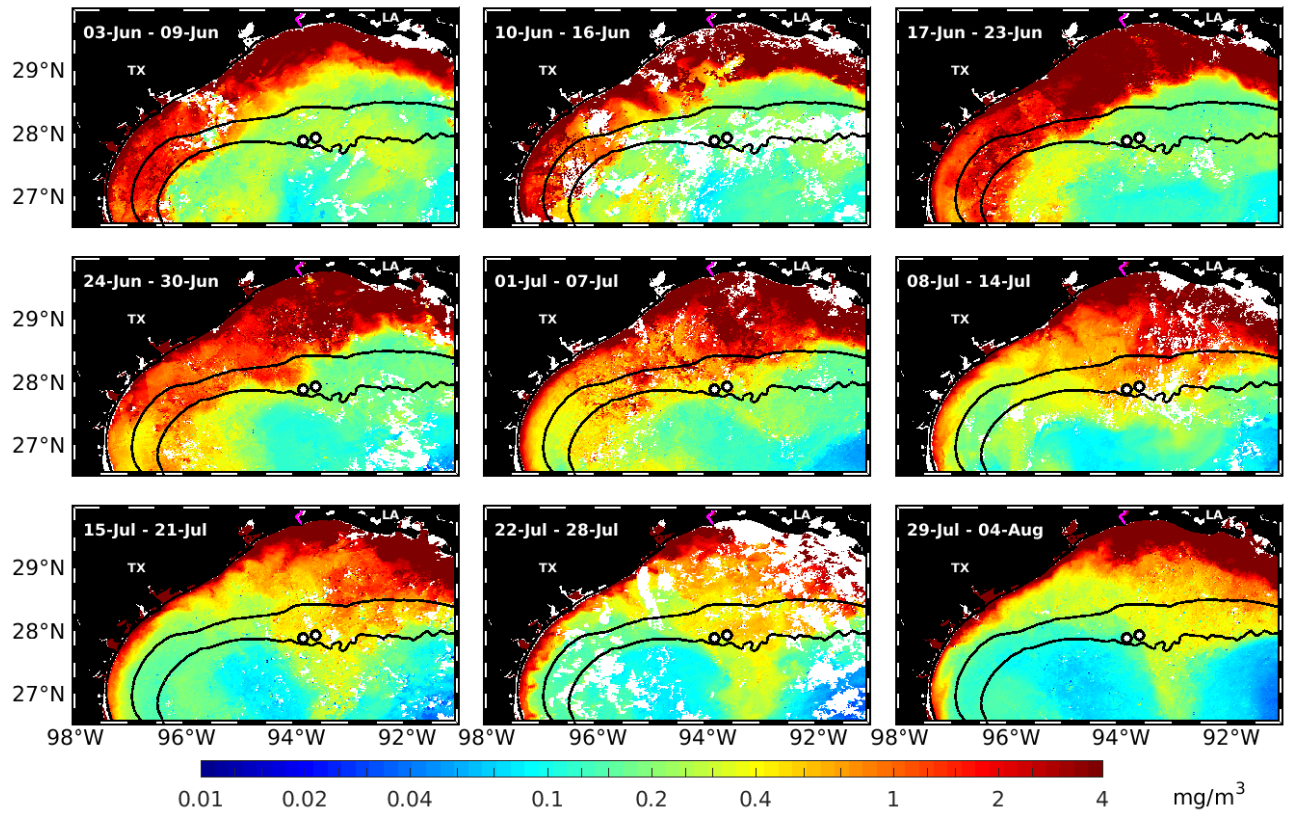
211 In addition to observations, we used outputs from a numerical simulation to investigate
212 certain aspects of the ocean conditions in June and July 2016. We examined hindcasts from our
213 data assimilative, 2 km (1/50°) resolution simulation of the full GoM with the HYbrid
214 Coordinate Ocean Model (GoM-HYCOM 1/50), which has 32 vertical levels (Le Hénaff and
215 Kourafalou, 2016; Androulidakis et al., 2019). The hybrid vertical coordinate system of
216 HYCOM makes it suitable for representing the regional circulation in areas comprising wide
217 continental shelves as well as the deep ocean, such as the GoM (Bleck, 2002;
218 <https://hycom.org/>). The GoM-HYCOM 1/50 simulation is forced with daily river discharges,
219 implemented at 22 major river mouth locations along the U.S. coasts, including along Texas,
220 while monthly climatological river discharges are represented at minor river mouth locations.
221 The simulation includes detailed representation of river plume dynamics, following Schiller
222 and Kourafalou (2010), and has been used to characterize the episodes of long-distance export
223 of the Mississippi River plume in 2014 (Le Hénaff and Kourafalou, 2016) and in 2015
224 (Androulidakis et al., 2019). The model assimilates satellite altimetry and SST data, as well as
225 available *in situ* data, in particular salinity and/or temperature profiles from Argo floats and
226 expendable Bathy Thermographs (XBT). The simulation is nested at open boundaries into the
227 operational global HYCOM simulation (GLB-HYCOM, hycom.org), and is forced at the
228 surface by the 3-hourly fields from the operational 0.125° resolution ECMWF atmospheric
229 simulation.

230

231 **3. Results**

232 After the FGB Sanctuary staff contacted us shortly after divers reported the mortality
233 event, we examined the series of apparent Chl-a images to analyze how the spatial patterns of
234 turbid coastal and clear offshore ocean waters changed over time, prior to and during the event.

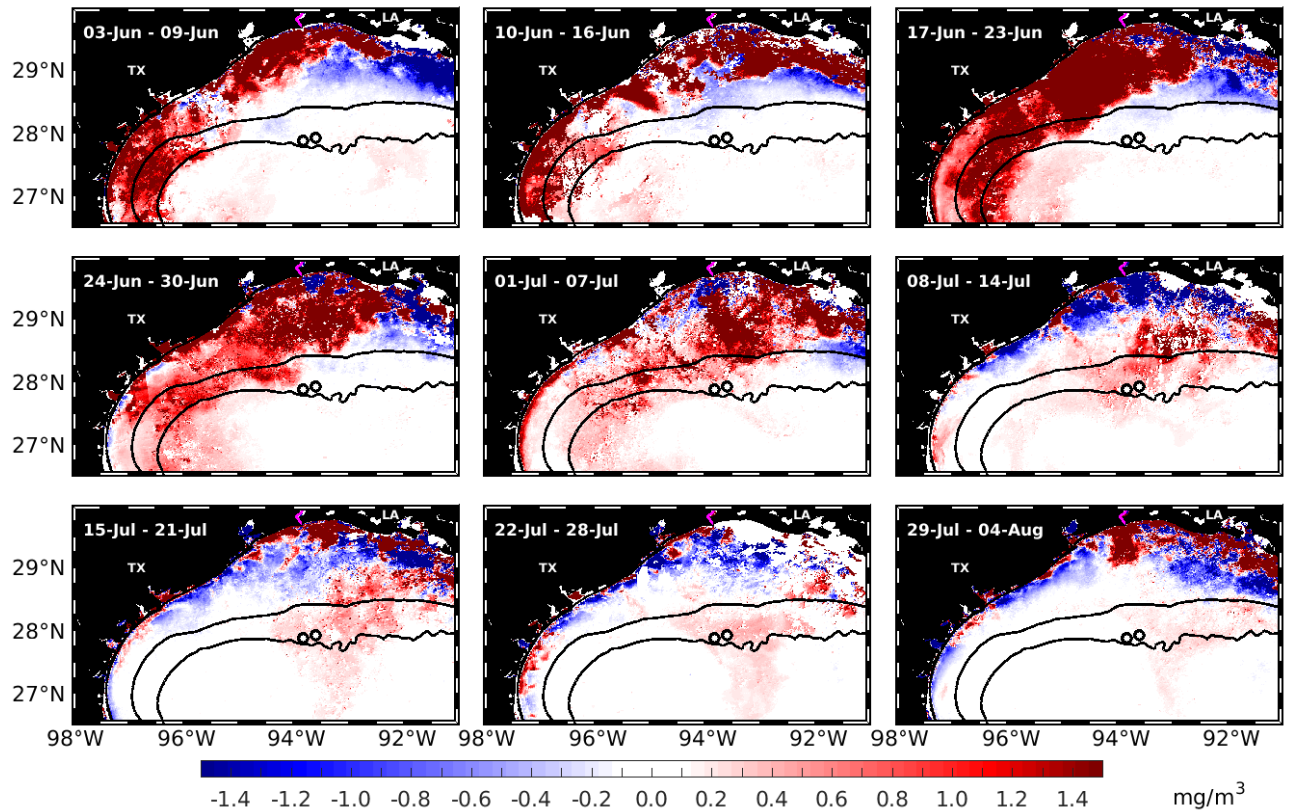
235 Leading up to the event, weekly composites of apparent Chl-a images show large
236 quantities of high apparent Chl-a waters along the NWGoM coast throughout June 2016 (Figure
237 2). During June 3-9, a wide band (~130 km) of high apparent Chl-a extended along the entire
238 coast of Texas. This pattern is not typical for this time of the year, as shown by the positive
239 anomalies in apparent Chl-a with respect to the 2003-2010 climatology (Figure 3). Along the
240 coast of Louisiana, in the northeast part of the domain, a narrow band (~60 km) of high apparent
241 Chl-a was observed on these dates (Figure 2). However, this band was associated with negative
242 apparent Chl-a anomalies (Figure 3), meaning that the apparent Chl-a was lower than the
243 climatological values in June 2016. This latter pattern also occurred in May 2016 (not shown),
244 suggesting that the Mississippi and Atchafalaya Rivers (in orange and red on Figure 1) had only
245 a limited influence in this area in the spring of 2016, compared to previous years.



246

247 *Figure 2: Temporal evolution of the offshore extension of surface brackish waters using*
 248 *Chlorophyll-a. Weekly composites of the apparent Chlorophyll-a concentration (Chl-a, mg/m³)*
 249 *from MODIS-Aqua from June 3-9 to July 29 - August 4, 2016. The black contours represent the*
 250 *isobaths at 50 and 200 m. The white circles with black outlines indicate the locations of the*
 251 *East and West FGB sites. The state border between Louisiana (LA) and Texas (TX) is indicated*
 252 *with a magenta line.*

253



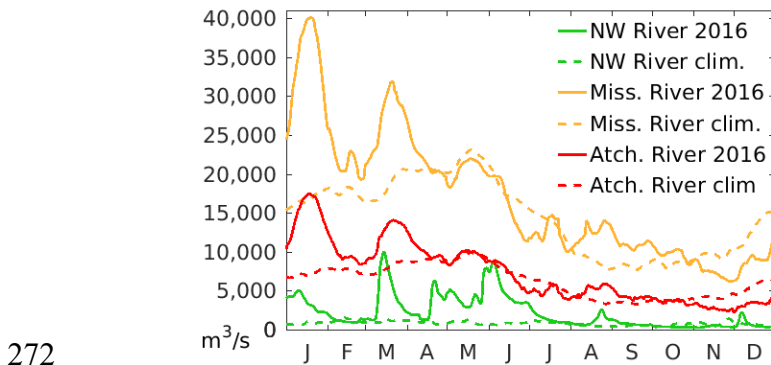
254

255 *Figure 3: Temporal evolution of the offshore extension of surface brackish waters using*
 256 *Chl-a anomalies. Weekly composites of apparent Chl-a anomaly with respect to the 2003-2010*
 257 *climatology (mg/m^3) from MODIS-Aqua from June 3-9 to July 29 - August 4, 2016. The black*
 258 *contours represent the isobaths at 50 and 200 m. The white circles with black outlines indicate*
 259 *the locations of the East and West FGB sites. The state border between Louisiana (LA) and*
 260 *Texas (TX) is indicated with a magenta line.*

261

262 The unusual spatial distribution of coastal river waters in the spring of 2016 off Texas
 263 is in part explained by the time series of river discharge in the region (Figure 4). Although the
 264 discharge of the Mississippi and Atchafalaya Rivers was high in the first quarter of 2016, these
 265 rivers showed lower discharge in the ensuing spring and summer, close to or below
 266 climatological values. On the other hand, the smaller rivers discharging into the NWGoM (in

267 green on Figure 1) showed sustained and large discharge values from April to June, with
 268 combined peak values near 10,000 m³/s, or 5 to 10 times larger than usual. This was the result
 269 of the intense local rains and floods that occurred during this period (Breaker et al., 2016). The
 270 cumulative discharge of these rivers in early June was equivalent to the discharge of the
 271 Atchafalaya River, and half of the Mississippi River discharge, for this time period.



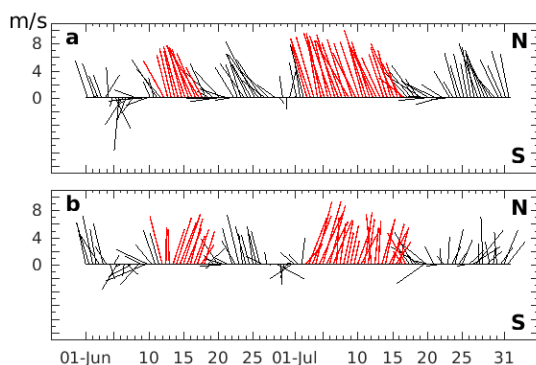
272
 273 *Figure 4: Temporal evolution of river discharge in the northern Gulf of Mexico in 2016.*
 274 *2016 river discharge time series (m³/s) for the combined northwestern Gulf of Mexico rivers in*
 275 *green (Sabine, Neches, Village Creek, Trinity, San Jacinto, Brazos, Lavaca, Guadalupe, and*
 276 *San Antonio rivers), the Mississippi River in yellow, and the Atchafalaya River in red. Solid*
 277 *lines show 2016 values; dashed lines show climatological values (2004-2014).*

278
 279 Between June 3-9 and June 17-23, the broad band of high apparent Chl-a along the Texas
 280 coast expanded offshore (Figure 2). During June 17-23, the brackish waters covered roughly
 281 two thirds of the distance between the Texas coast and the FGB. In the following 7-day period,
 282 from June 24 to 30, the band of high apparent Chl-a waters continued extending offshore and
 283 almost reached the FGB sites from the northwest (Figure 2).

284 During July 1-7 and July 8-14, the high apparent Chl-a waters reached the FGB area.
 285 Apparent Chl-a values along the coast of the LATEX shelf decreased markedly at this time

286 (Figures 2 and 3). Indeed, the large pool of coastal, turbid waters observed there in June had
 287 been advected offshore, reaching the FGB. After July 8-14, the apparent Chl-a at the edge of
 288 the shelf break around the FGB decreased, but the FGB sites remained affected with high
 289 apparent Chl-a until July 29 – August 4 (Figures 2 and 3). By that time, the high apparent Chl-
 290 a event that affected the FGB had subsided (Figure 3).

291 Figure 5 presents the wind vectors for June and July 2016 at two buoys located on the
 292 LATEX shelf (see Figure 1). The vector plots show two episodes of sustained upwelling-
 293 favorable winds along the coast. These two periods are highlighted in red. First, from June 12
 294 to 18, southerly winds blew along the southern coast of Texas adjacent to Mexico ($\sim 27^\circ\text{N}$,
 295 $\sim 96.5^\circ\text{W}$, Figure 5a), i.e. almost parallel to the coast at that location (Figure 1). This favored
 296 eastward, offshore export of coastal waters through Ekman transport (Zavala-Hidalgo et al.,
 297 2006). Within two days, intense southwesterly winds also blew in the region off Galveston
 298 ($\sim 29^\circ\text{N}$, $\sim 94.5^\circ\text{W}$, Figure 5b), almost parallel to the coast, thus also favoring upwelling there.
 299 This wind event coincided with the initial offshore export of turbid coastal waters (Figures 2
 300 and 3). Analysis of the daily apparent Chl-a images shows that, from June 10 to June 16, the
 301 offshore front of the coastal waters advanced ~ 50 km over 6 days, or an average ~ 0.1 m/s.



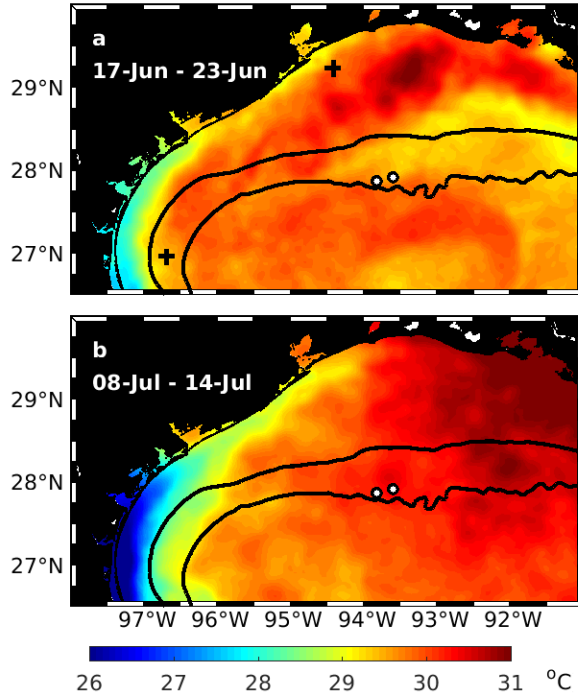
302
 303 *Figure 5: Wind conditions along the Texas coast in June and July 2016. (a) 10-m wind*
 304 *vectors (m/s) at NDBC station 42020 located at (26.97°N; 96.67°W) every 12 hours for June*
 305 *and July 2016. In red are the wind vectors in June 12-18 and July 2-17, during the upwelling*

306 *events (see text). (b) same as (a) at the NDBC station 42035 located at (29.23°N; 94.41°W).*
307 *The upward direction is the north (marked with N), the downward direction is the south*
308 *(marked with S).*

309

310 In July, intense, sustained winds were observed at both NWGoM stations for the first
311 half of the month (from July 2 to 17), with the most intense winds in the July 3-10 period. Like
312 in June, these were dominantly southerly along southern Texas, and southwesterly off
313 Galveston, so that the winds were upwelling-favorable along the entire Texas coast. These
314 winds thus also favored the offshore advection of the turbid, brackish coastal waters. By mid-
315 July, apparent Chl-a values along the coast of the LATEX shelf decreased markedly (Figures 2
316 and 3) as the large pool of coastal, turbid waters observed there in June had been advected
317 offshore. Between July 2 and July 4, the front moved rapidly, over ~40 km, corresponding to a
318 ~0.2 m/s velocity. Then, the leading front of coastal waters slowed down, but still advanced an
319 additional ~40 km through July 12. On average, between July 2 and July 12, the front advanced
320 at ~0.1 m/s.

321 The upwelling in mid-June and early July 2016 was confirmed by examination of the
322 weekly satellite-derived SST observations (Figure 6). Although upwelling is common in
323 summer in the western GoM (Zavala-Hidalgo et al., 2006), the events described here led to
324 especially widespread cool sea surface temperatures, particularly in July 2016, extending from
325 Mexico as far as Galveston Bay (Figure 6b). The coastal upwelling of June and July 2016 led
326 to the offshore advection of the river waters that had accumulated along the coast in the spring
327 of 2016.



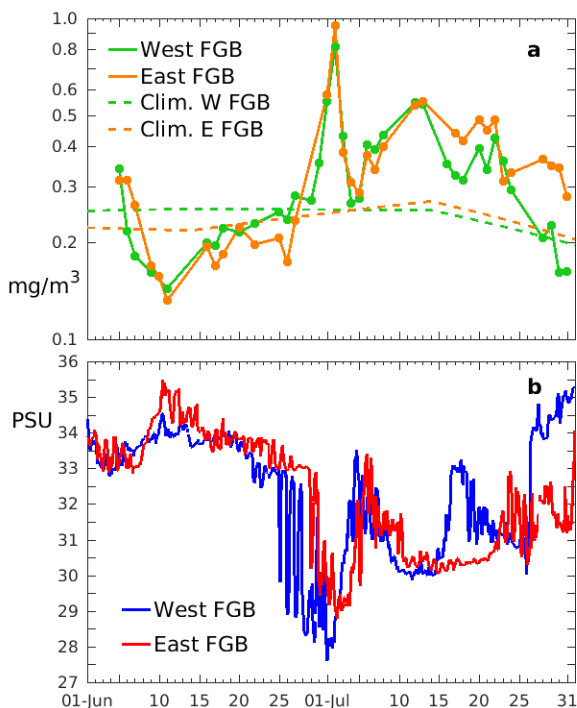
328

329 *Figure 6: Evidence of upwelling along the Texas coast in June and July 2016 based on*
 330 *Sea Surface Temperature maps. Weekly averages of Sea Surface Temperature (°C) from the*
 331 *GHRSSST dataset for: (a) June 17-23; (b) July 8-14, 2016. The black contours represent the*
 332 *isobaths at 50 and 200 m. The white circles with black outlines indicate the locations of the*
 333 *East and West FGB sites. The black crosses near the coast indicate the locations of the*
 334 *meteorological NDBC buoy stations 42020 and 42035 (see also Figure 1).*

335

336 We now focus on the detailed timeline of the influence of coastal river waters on the
 337 FGB. Figure 7a presents the time series of the surface apparent Chl-a levels above both FGB
 338 sites, derived using the daily instantaneous estimates from MODIS (Aqua and Terra) and
 339 VIIRS, as well as climatological apparent Chl-a values. We checked that the observations from
 340 each satellite source were consistent with one another during our study period before blending
 341 them into a single, multi-sensor apparent Chl-a time series. The time series provided
 342 exceptional coverage, in complement to the weekly composites shown in Figures 2 and 3. In

343 particular, it shows that the largest apparent Chl-a values above the FGB were reached on July
 344 2nd, when the front of turbid brackish waters reached the FGB locations for the first time. The
 345 peak in surface apparent Chl-a values is short, and apparent Chl-a values decreased over the
 346 following days. Before the peak, in June, the values at both sites were lower than the
 347 climatological values. After the peak, the apparent Chl-a values remained higher than
 348 climatological values, and increased again after July 5. The values of surface apparent Chl-a at
 349 both FGB sites were similar throughout June and July until July 13. After July 13, surface
 350 apparent Chl-a at East FGB was larger than at West FGB until the end of July. Between July
 351 13 and 22, surface apparent Chl-a at East FGB reached 0.4 to 0.5 mg/m³, more than twice the
 352 climatological value, in the period directly preceding the observation of the mortality. The
 353 positive surface apparent Chl-a for this period was smaller than the one around July 2 but it
 354 lasted longer at East FGB.



355
 356 *Figure 7: Signature of the presence of surface brackish waters at the FGB locations. (a)*
 357 *Time series of apparent Chl-a (mg/m³) at the surface above the West FGB site (green) and the*

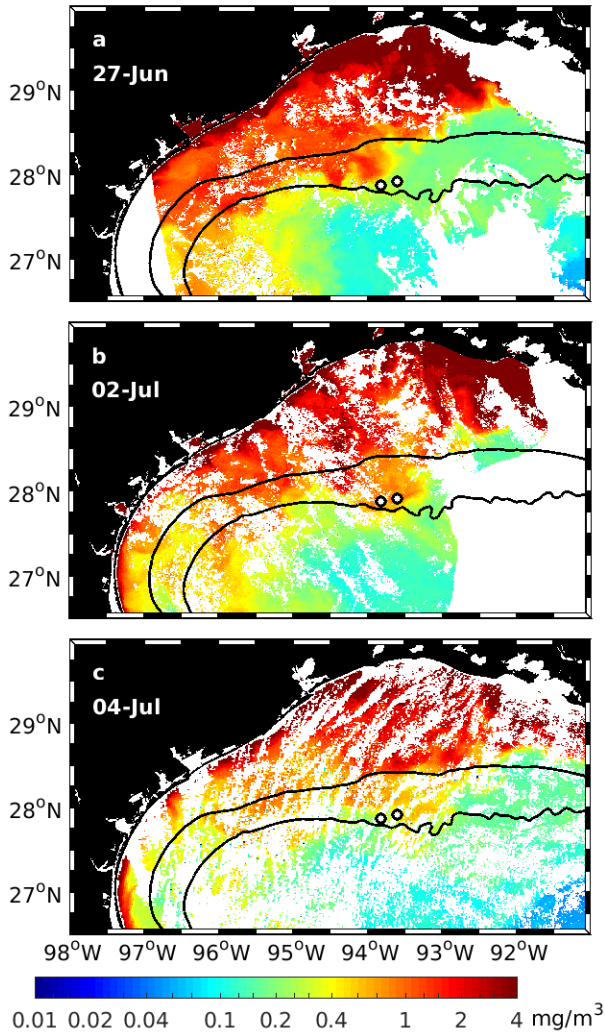
358 *East FGB site (orange) in June and July 2016, based on MODIS Aqua, MODIS Terra, and*
359 *VIIRS (solid lines). The 2003-2010 climatological monthly values (mg/m^3) estimated from*
360 *MODIS-Aqua are indicated for reference (dashed lines). (b) Time series, in June and July 2016,*
361 *of surface salinity (PSU) above the West FGB site (blue) and the East FGB site (red) from the*
362 *TABS buoy data.*

363

364 Figure 7b presents the hourly surface salinity observed above both East and West FGB
365 sites. These observations are consistent with the surface apparent Chl-a time series (Figure 7a).
366 Low salinity waters reached both the East and West FGB locations in late June, with a peak
367 around July 2. Surface salinity in late June and early July was lower at West FGB than at the
368 East FGB, and the influence of coastal waters lasted longer at West FGB than at East FGB
369 during that period. After July 2nd, the salinity time series show, like for the surface apparent
370 Chl-a, a decrease of the influence of coastal waters, marked with an increase in salinity at both
371 sites, before a second period of influence of coastal waters. As for the apparent Chl-a, that
372 second period is less marked than the one around July 2nd, but it lasted longer at East FGB.
373 From July 10 to 22, the surface salinity at East FGB remained constantly below 31, indicating
374 a prolonged period of presence of the brackish coastal waters atop the East FGB.

375 Figure 8 illustrates the spatial patterns in apparent Chl-a observed in late June and early
376 July 2016, when the first peak in apparent Chl-a was observed above both East and West FGB
377 sites (Figure 7). On June 27 (Figure 8a), the band of coastal waters, which had been extending
378 from the coast (Figure 2), formed a bulge extending southeastward, reaching close to the FGB
379 sites and partially affecting the West FGB site (Figure 7b). On July 2 (Figure 8b), this bulge
380 extended further southeastward and covered both FGB sites. On July 4 (Figure 8c), it had
381 recessed and the apparent Chl-a at FGB sites was lower than in the waters to the north and east

382 of the sites. These patterns explain the short peak observed in surface apparent Chl-a on July 2
383 (Figure 7a) at both FGB sites.

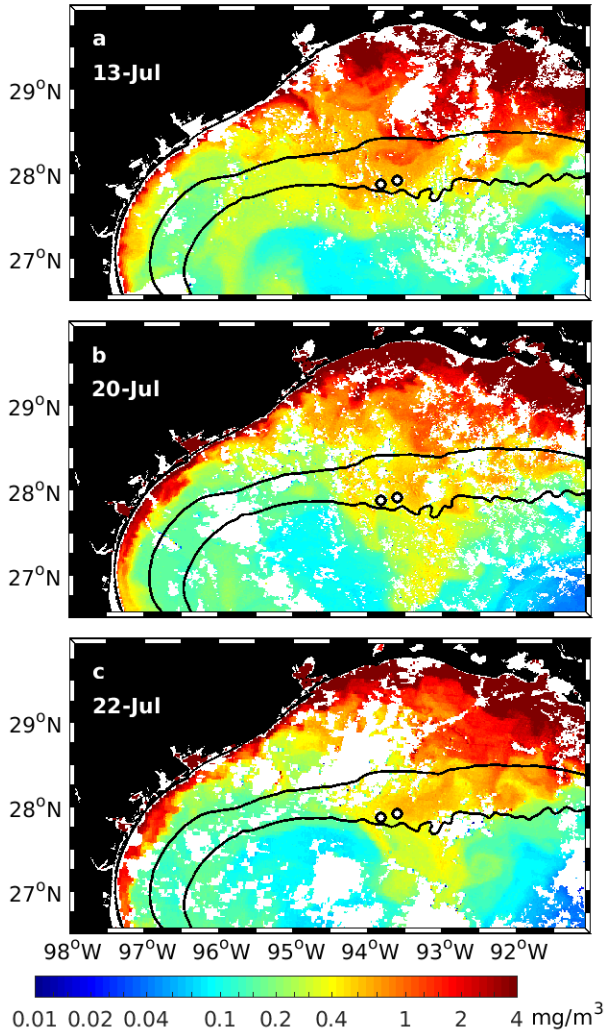


384

385 *Figure 8: Spatial patterns in surface apparent Chl-a observed during the first*
386 *Chlorophyll-a peak observed above both East and West FGB sites in late June and early July*
387 *2016. Apparent Chl-a (mg/m³) observed on: (a) June 27, 2016 at 18:05 UTC by MODIS-Aqua,*
388 *(b) July 2, 2016, at 15:15 UTC by MODIS-Terra, and (c) July 4, 2016, at 16:40 UTC, by*
389 *MODIS-Terra. The black contours represent the isobaths at 50 and 200 m. The white circles*
390 *with black outlines indicate the locations of the East and West FGB sites.*

391

392 Figure 9 provides more details about the situation in mid to late July. On July 13 (Figure
393 9a), the surface plume of coastal waters covered the central and eastern parts of the LATEX
394 shelf and its southward extension covered both FGB sites. Within these coastal waters, a
395 filament of more intense apparent Chl-a was located just north of the East FGB site. On July
396 20 (Figure 9b), the spatial distribution of the coastal waters in the NWGoM was similar,
397 although apparent Chl-a was somewhat lower relative to July 13. A portion of the coastal, high
398 apparent Chl-a waters was also entrained south of the FGB to the deep GoM. Waters with larger
399 apparent Chl-a were located to the north and northeast of the East FGB site, which explains the
400 larger surface apparent Chl-a and lower salinity at East FGB than at West FGB at that time
401 (Figure 7). This pattern is more visible on July 22 (Figure 9c), when a patch of higher apparent
402 Chl-a covered the East FGB site but not the West site. The maps of apparent Chl-a explain the
403 higher surface apparent Chl-a and lower salinity at the East FGB site than at the West FGB site
404 during July 13-22 (Figure 7).



405

406

407

408

409

410

411

412

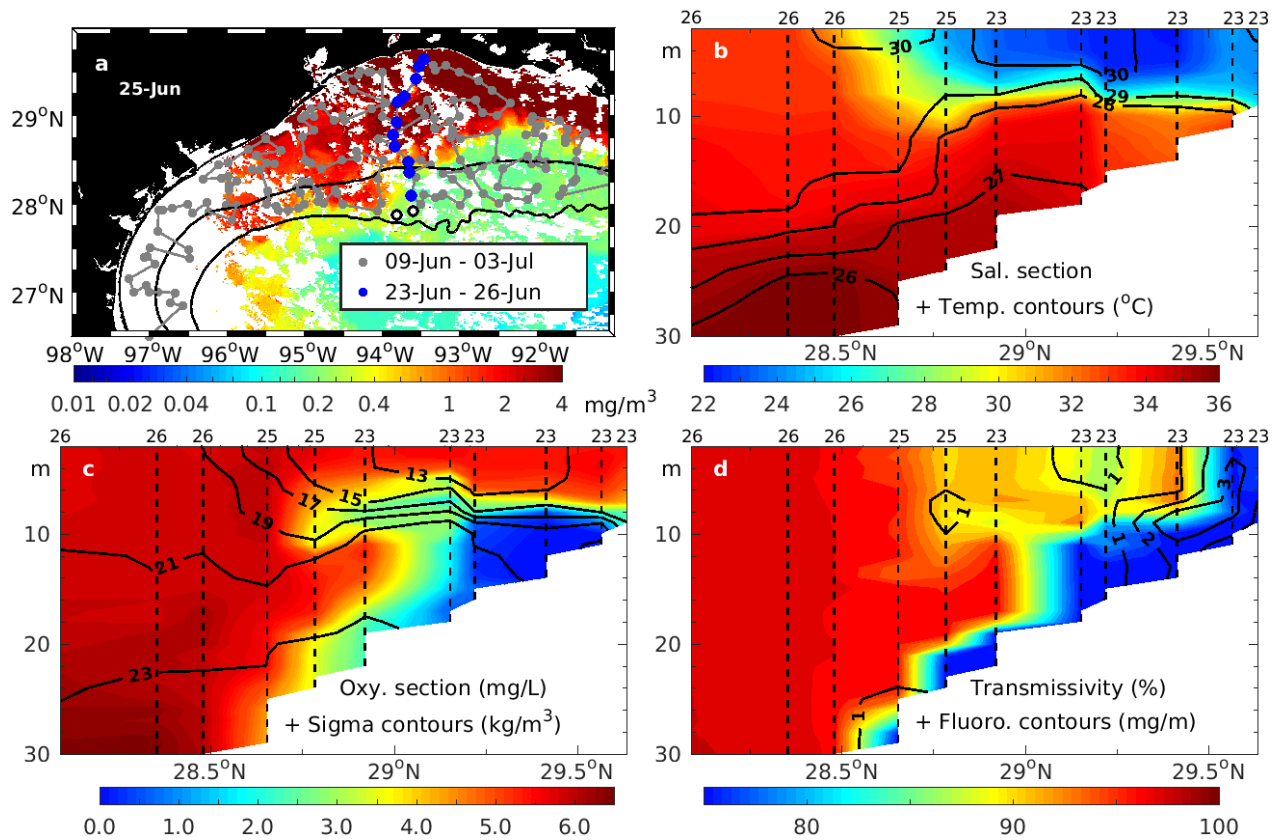
413

414

Figure 9: Spatial patterns in surface apparent Chl-a observed during the second Chlorophyll-a peak observed above the FGB sites in mid to late July 2016. Apparent Chl-a (mg/m^3) observed by MODIS-Terra on: (a) July 13, 2016 at 16:35 UTC, (b) July 20, 2016, at 16:40 UTC, and (c) July 22, 2016, at 16:30 UTC. The black contours represent the isobaths at 50 and 200 m. The white circles with black outlines indicate the locations of the East and West FGB sites.

We now investigate the vertical structure of the upper ocean over the LATEX shelf, by analyzing the *in situ* observations of salinity, temperature, density, dissolved oxygen, and

415 chlorophyll concentration in the water column, collected by the R/V *Oregon II* in June 2016
 416 (Figure 10). A hydrographic section centered at about 93.7°W, east of Galveston Bay
 417 (~94.5°W), was constructed from samples collected during June 23-26 (blue dots in Figure
 418 10a). That section was constructed artificially by using data collected from the ship over a 3-
 419 day period. Since the maximum velocity of the surface coastal water front in June was estimated
 420 to be ~0.1 m/s, this corresponds to a maximum displacement of the front of ~26 km during the
 421 three-day observation period, which is much smaller than the total length of the section (189
 422 km). We are thus confident that this section represents a near synoptic view of the vertical
 423 structure through the plume of coastal waters.



424
 425 *Figure 10: Evidence of a mid-water layer of low oxygen waters extending offshore in*
 426 *the NWGoM in June 2016. (a) Apparent Chl-a (mg/m³) observed by MODIS-Aqua on June 25,*
 427 *2016 at 18:20 UTC. Superimposed are the locations of the in situ samples from the R/V Oregon*
 428 *II collected from June 9 to July 3, 2016. The blue dots represent a virtual track constructed*

429 *from stations of the actual cruise track (in grey dots and lines) occupied between June 23-26.*
430 *The black contours represent the isobaths at 50 and 200 m. The white circles with black outlines*
431 *indicate the locations of the East and West FGB sites. (b-d) Vertical sections, along the virtual*
432 *track (blue dots) shown in (a), of: (b) salinity (colors) and temperature (contours, °C), (c)*
433 *dissolved oxygen (colors, mg/L) and sigma density anomalies (contours, kg/m³), (d)*
434 *transmissivity (colors, %) and chlorophyll fluorometry (contours, mg/m). (b-d) The vertical*
435 *sections are linearly interpolated between the individual vertical profiles collected during the*
436 *cruise. The vertical dashed black lines mark the locations of in situ measurements. The day of*
437 *the month (June) at which these measurements were taken is marked at the top of each vertical*
438 *dashed line.*

439

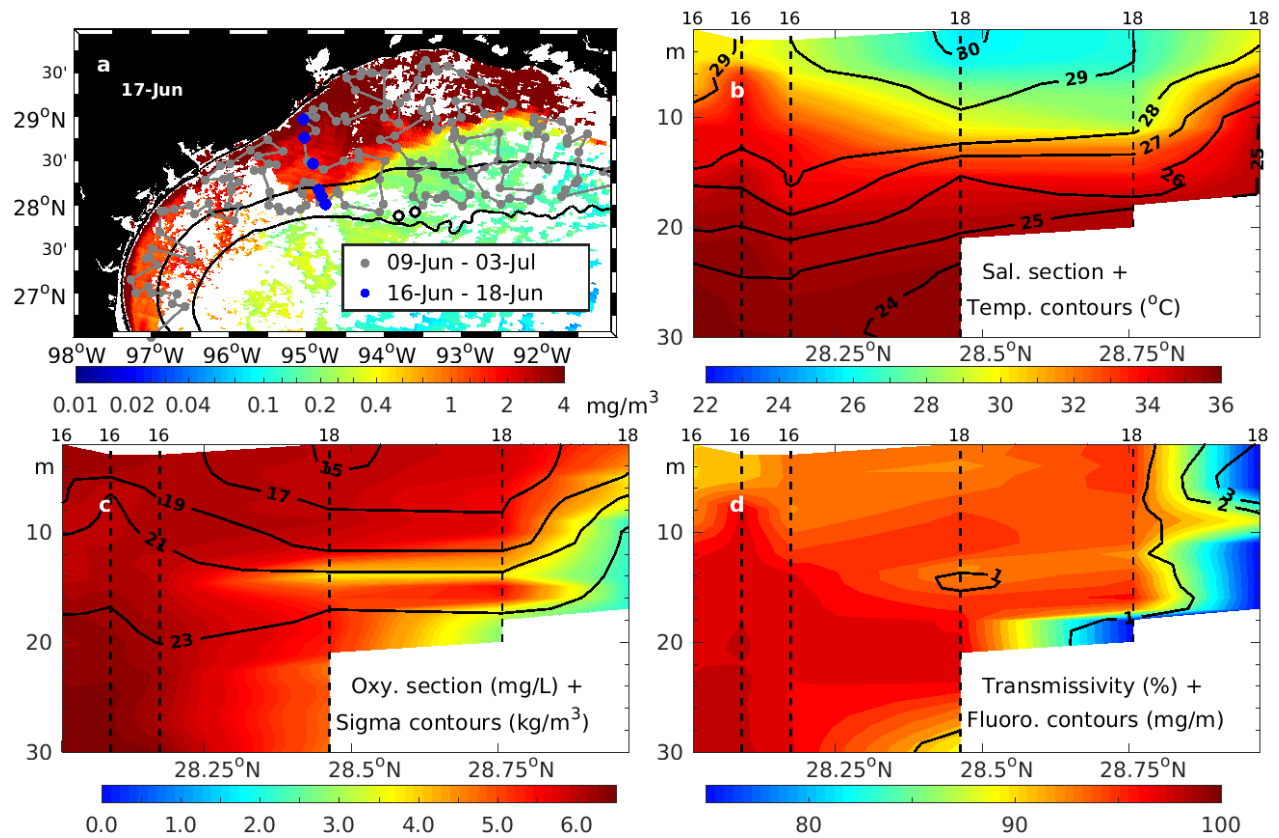
440 The hydrographic section spans the initial offshore expansion of the turbid coastal river
441 plume following the mid-June upwelling. The cross-shelf section of salinity and temperature
442 (Figure 10b) shows a brackish water plume extending from the surface to 5-10 m depth, and
443 from the coast southward to about 28.5°N. This agrees with the front of high apparent Chl-a
444 observed in the satellite data (Figure 10a). Salinity within the brackish water layer was as low
445 as 22. A marked density gradient (Figure 10c, contours) was observed at the bottom of the
446 buoyant plume. Figure 10c shows a marked dissolved oxygen deficit immediately below the
447 surface layer of brackish waters, which are marked with low salinity and high apparent Chl-a.
448 Dissolved oxygen values in the subsurface tongue spreading offshore were <3 mg/L (hypoxic
449 waters are usually defined with values <2 mg/L). Outside this thin layer, values were larger
450 than 6 mg/L.

451 Layers of dissolved oxygen minima are not uncommon below a river plume. These are
452 typically observed in the large hypoxic region of the northern GoM on the LATEX shelf in

453 summer. Zhang et al. (2015) observed such mid-water oxygen minimum layers south of
454 Atchafalaya Bay (~92°W) and south of the Mississippi Delta extending offshore 20 to 25 km.
455 They show that such low oxygen layers can be continuous and that they track the bottom
456 boundary layer, where the pycnocline intersects the bottom. The low oxygen layers basically
457 detach from the bottom layer and follow the pycnocline offshore.

458 In June 2016, the mid-water layer of low dissolved oxygen extended southward 30 to
459 40-km, reaching 100 km from the coast. This is further offshore than had previously been
460 observed in the NWGoM by Zhang et al. (2015, ~65 km). This low oxygen layer was associated
461 with high turbidity (low light-transmission) and high relative chlorophyll fluorescence. Its
462 position, immediately below the surface plume of brackish waters (Figure 10d) indicates that
463 particles containing chlorophyll were sinking from the surface plume and accumulating at the
464 pycnocline. Phytoplankton and other associated organic particles sink and become trapped in
465 such density layers. Unable to photosynthesize in the dark under the plume, the phytoplankton
466 decomposed along with organic matter advected from the coast. This bacterial activity led to
467 the low oxygen observed.

468 A similar low oxygen layer below the surface brackish plume was observed along a
469 second near-synoptic section from the R/V *Oregon II* cruise around ~94.9°W, southwest of
470 Galveston Bay, between June 16 and 18 (Figure 11). There, the low-salinity surface layer
471 extended to 10-15 m depth, with a salinity value of 26. Below this surface layer, a very thin
472 layer of low oxygen, with values as low as 3.5 mg/L, extended offshore over a 30 to 40 km
473 distance. This layer was also associated with low light transmission and high chlorophyll
474 fluorescence.



475

476 *Figure 11: Same as Figure 10, for the virtual section indicated in blue dots in (a), for*
 477 *data collected between 16-18, 2016. (a) Apparent Chl-a (mg/m³) observed by MODIS-Terra*
 478 *on June 17, 2016 at 16:00 UTC.*

479

480 The evidence of cross-shelf low oxygen mid-water layers under an eastward-
 481 southeastward propagating surface brackish layer over the LATEX shelf shows that such layers
 482 can form not only under the Mississippi/Atchafalaya plume, as observed previously (Zhang et
 483 al., 2015), but also under a surface layer to which small, local NWGoM rivers contributed
 484 significantly. This complements the identification of nearshore hypoxia forced by the Brazos
 485 river along the Texas coast (DiMarco et al., 2012).

486

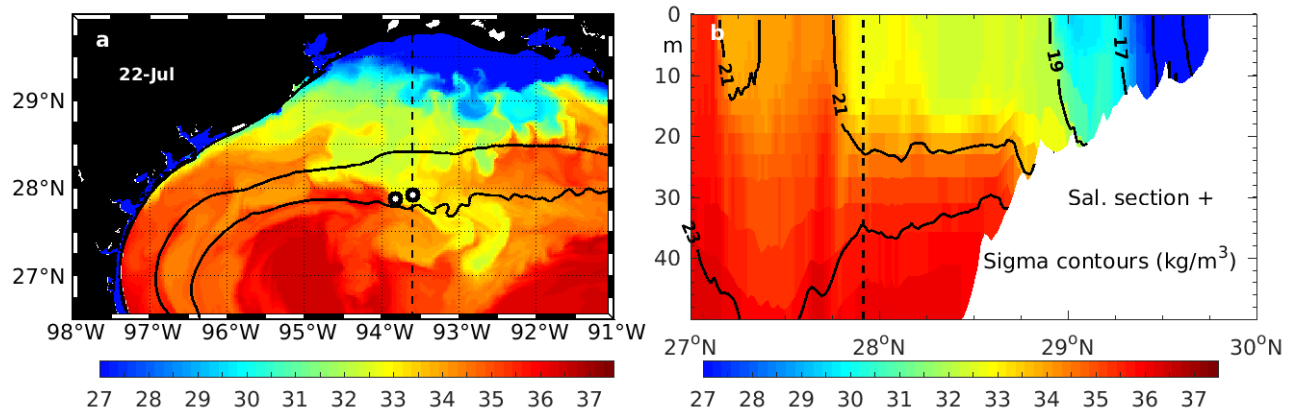
487 **4. Discussion and conclusions**

488 Our results confirm that the FGB mortality event of July 2016 occurred after the turbid
489 coastal waters, which accumulated in the spring of 2016 after precipitation and river discharge
490 excess along the Texas coast, were advected offshore by upwelling favorable winds. During
491 that process, as we just described, mid-water layers of low oxygen were observed to extend
492 about half-way on the shelf in June, which is remarkable. Such a mid-water layer of very low
493 oxygen values (hypoxic waters), comparable to the ones observed in June 2016, intersecting
494 the underwater reefs at FGB could be fatal to corals and sponges. However, the other vertical
495 profiles collected in June 2016 do not show the presence of these mid-water layers of low
496 oxygen, which suggests that these layers were patchy and localized. In addition, although these
497 mid-water layers extended far offshore on the LATEX continental shelf, their extent was still
498 another ~90 km away from the FGB sites. As the surface layer of brackish waters extended
499 further offshore, its bottom was more prone to being ventilated from below in open shelf
500 conditions, so that it is unlikely that the level of oxygen could be maintained at very low levels
501 as far offshore as the FGB sites. These considerations make it unlikely that a mid-water filament
502 of hypoxic waters directly impacted the East FGB.

503 However, the presence of mid-water layers of low oxygen so far offshore as observed in
504 June 2016 illustrates the very large quantities of organic matter that were entrained offshore,
505 which made the surface layer of brackish waters prone to developing a low-oxygen layer at its
506 base. As the surface layer of brackish waters reached the FGB seamounts, it found a portion of
507 seafloor at a shallow depth, ~23 m at East FGB (17 m is the shallowest part of the seamount,
508 23 m is the seafloor, Johnston et al., 2019).

509 In order to characterize the vertical extent of the brackish plume in July, at the period
510 when the mortality took place, we use outputs from the GoM-HYCOM 1/50 model simulation

511 (see Section 2), with realistic river forcing and data assimilation, on July 22, 2016 (Figure 12).
512 The simulated sea surface salinity (Figure 12a) shows very similar patterns as those observed
513 on apparent Chl-a on the same day (Figure 9c): first, the core of the brackish and fresh plume
514 is located on the northern part of the shelf, and the plume extends over the shelf to the south;
515 then, although their location slightly differs, both the observations and the simulation show
516 filaments of waters with stronger riverine signature (large apparent Chl-a or low salinity) just
517 north of the FGB sites; finally, filaments of low-salinity, riverine waters were exported south
518 of the shelf break near the FGB sites in the simulation, similar to observations. The salinity of
519 the surface waters reaching East FGB was ~ 33 in the simulation, compared to ~ 31 in the
520 observations on July 22 (Figure 7). Despite these differences, the simulation is able to represent
521 the offshore export of brackish waters in July 2016 over the NWGoM shelf in a realistic manner.
522 The vertical structure of the simulated brackish plume extended to ~ 20 m depth on the outer
523 part of the shelf, including in the FGB area (Figure 12b). This model estimate is in agreement
524 with limited observational data sampled on the LATEX shelf in July 2016, which show that the
525 low-salinity surface layer extended to ~ 20 m depth (S. DiMarco, personal communication). *In*
526 *situ* data from the U.S. Geological Survey showed low values of subsurface dissolved oxygen
527 at a couple sites on the LATEX shelf, at similar depths as the East FGB top, in late July and
528 early August 2016 (Johnston et al., 2019). These observations also suggest that the surface layer
529 of brackish waters extended to ~ 20 m depth; they also suggest that mid-water layers of low
530 oxygen were also present on the shelf in July 2016, stressing again the large quantities of
531 organic matter exported in the surface layer.



532

533 *Figure 12: Spatial and vertical extent of the simulated plume of brackish waters on July*
 534 *22, 2016. (a) Simulated sea surface salinity (PSU) on July 22. The black contours represent the*
 535 *isobaths at 50 and 200 m. The white circles with black outlines indicate the locations of the*
 536 *East and West FGB sites. (b) Vertical section (in m of depth), along the meridional dashed line*
 537 *at the longitude of East FGB shown in (a), of salinity (colors) and sigma density anomalies*
 538 *(contours, kg/m³). The vertical dashed line marks the location of East FGB.*

539

540 We expect that the presence of brackish waters just over the seamount cap led to the
 541 accumulation of organic matter on the seafloor. As is happening on the LATEX upper-shelf in
 542 summer, a layer of highly turbid waters present at the top of the seamount would be isolated
 543 between the seafloor and the strong stratification at the base of the surface, low-salinity waters.
 544 This would severely inhibit the ventilation of the bottom layer, favoring hypoxia (Rabalais et
 545 al., 2001, 2002). This process is consistent with the patterns of the mortality reported during
 546 the assessment dives in late July and early August 2016, with the affected organisms located at
 547 the base of coral structures and in sand channels between them (Johnston et al., 2019).

548 In addition to the shallow seafloor at the top of the FGB seamounts, coral structures at
 549 the top of the seamounts themselves might also have favored retention of organic matter.

550 Indeed, immersed corals are often seen as a canopy that slows down the current near the bottom,
551 especially under limited wave influence as expected at the depth of the FGB sites (Nepf and
552 Vivoni, 2000; Nepf, 2012; Lowe and Falter, 2015; Pomeroy et al., 2017). Moreover, large coral
553 structures were also found to slow the current at their base, which favored coral bleaching in
554 lagoons of Moorea, French Polynesia (Lenihan et al., 2008). In general, low-velocity flow
555 conditions around corals favor bleaching (Nakamura and van Woesik, 2000; Nakamura et al.,
556 2005) and hypoxia (Brown and Carpenter, 2013). The coral structures at the top of the East
557 FGB, as they tend to reduce the velocity of the flows near the seafloor, thus favored the
558 accumulation of organic matter deposited from the surface brackish waters. Although it is not
559 possible, with the existing data, to confirm that such small-scale dynamical processes played a
560 significant role at East FGB, they might also have contributed to the local formation of low
561 oxygen waters.

562 The time series of surface apparent Chl-a and salinity above both FGB sites (Figure 7)
563 and the evolution of the spatial extent of the surface layer of coastal waters (Figure 9) might
564 explain why the East FGB site was the only one affected. Indeed, surface apparent Chl-a values
565 were larger, and salinity was lower, at East FGB than at West FGB for a prolonged period of
566 time between July 13 and 22 (Figure 7). This indicates that the presence of river waters was
567 more marked at East FGB site compared to West FGB, which suggests that: 1) the stratification
568 at the base of the surface layer was more intense; 2) the organic matter content was higher. Both
569 processes make the local formation of a low oxygen layer at the top of the East FGB seamount
570 more likely than at the West FGB site.

571 The fact that the presence of brackish waters at both FGB sites in late June/early July,
572 with more pronounced anomalies in apparent Chl-a and salinity than later in July, did not lead
573 to mortality might be due to the duration of that initial peak, which was shorter than the one in
574 mid-July. During laboratory experiments, Altieri et al. (2017) found that corals exposed to

575 hypoxic conditions died in less than 7 days, while Haas et al. (2014) observed complete coral
576 mortality of corals in hypoxic conditions in about 3 days. Whereas the initial peak in late
577 June/early July might have led to hypoxic conditions, they might not have prevailed for a long
578 enough time to lead to mortality, whereas the prolonged presence, at East FGB, of the brackish
579 waters from July 10 to 22 appears more favorable.

580 The absence of mortality during the short presence of brackish waters in late June/early
581 July might also be due to dynamical conditions, as quiescent conditions would likely be
582 necessary to retain the organic matter at the top of the seamount. Such quiescent conditions
583 might have been favored by the coral structures at the top of the FGB sites. A high-resolution,
584 coupled physics-biogeochemistry model, with adapted drag coefficient on the top of the
585 seamount to represent the effect of the corals, will be necessary to further study the physical
586 and biogeochemical processes that led to the coral mortality at East FGB.

587 The offshore export of low-salinity, riverine waters over the NWGoM continental shelf,
588 which we describe in detail in the Results section, thus provided favorable conditions for the
589 local formation of a layer of low-oxygen waters at the top of the East FGB seamount, which
590 were reported to be the most likely contributing factor in the reported mortality of corals and
591 sponges (Johnston et al., 2018). The expansion, in the summer of 2016, of riverine waters on
592 the NWGoM shelf over such a wide area was exceptional. The event was associated with the
593 extremely large amount of fresh water discharged by small Texas rivers onto the NWGOM
594 shelf in early summer 2016, which was due to unusually high precipitation in spring. This
595 extreme precipitation in 2016 followed intense precipitation in 2015, which was also associated
596 with large river discharge into the GoM (Fournier et al., 2016), although no distant hypoxia was
597 reported that year.

598 The results presented here help understand the anomalous coral and sponge mortality
599 event of 2016 at FGB. As high local precipitation, combined with winds favoring the offshore
600 transport of coastal waters, can episodically occur, our study findings should be beneficial to
601 the design of future monitoring plans. Moreover, these findings suggest that similar processes
602 might affect other coral reefs worldwide, especially those located near known hypoxic zones
603 (Altieri et al., 2017). Coastal freshwater discharge conditions and the variability of the plumes
604 they generate should be monitored routinely to differentiate between various processes that
605 impact the health of coral reef ecosystems, even those at large distances from the coast.

606

607 **Acknowledgements**

608 This paper is a result of research funded by the National Oceanic and Atmospheric
609 Administration's RESTORE Act Science Program under award NA15NOS4510226 to the
610 University of Miami. It is a contribution to the Marine Biodiversity Observation Network
611 (MBON) program. The work was partially supported by NASA grant NNX14AP62A 'National
612 Marine Sanctuaries as Sentinel Sites for a Demonstration Marine Biodiversity Observation
613 Network (MBON)' funded under the National Ocean Partnership Program (NOPP RFP NOAA-
614 NOS-IOOS-2014-2003803 in partnership between NOAA, BOEM, and NASA), and the
615 NOAA Integrated Ocean Observing System (IOOS) Program Office. M. Le Hénaff received
616 partial support for this work from the base funds of the NOAA Atlantic Oceanographic and
617 Meteorological Laboratory and was supported in part under the auspices of the Cooperative
618 Institute for Marine and Atmospheric Studies (CIMAS), a cooperative institute of the
619 University of Miami and NOAA, cooperative agreement NA10OAR4320143. The
620 Chlorophyll-a data were derived from ocean color images collected by the NASA Moderate
621 Resolution Imaging Spectroradiometer (MODIS), were obtained from NASA's Ocean Biology

622 Processing Group, and were further processed and distributed by the University of South
623 Florida's Institute for Marine Remote Sensing (<http://data.imars.marine.usf.edu>). The MUR
624 Global High-Resolution SST dataset is distributed by NASA
625 (<http://podaac.jpl.nasa.gov/dataset/JPL-L4UHFnd-GLOB-MUR>). The NOAA National Data
626 Buoy Center data are publicly available (www.ndbc.noaa.gov). The river discharge data from
627 USGS and the Army Corps of Engineers are distributed by the Gulf of Mexico Coastal Ocean
628 Observing System (GCOOS, [http://gcoos.tamu.edu/products/index.php/waterquality/river-](http://gcoos.tamu.edu/products/index.php/waterquality/river-discharge-data/)
629 [discharge-data/](http://gcoos.tamu.edu/products/index.php/waterquality/river-discharge-data/)). The R/V *Oregon II* cruise in June 2016 was supported by a collaboration
630 between the NOAA National Marine Fisheries Service (NMFS) and the Southeast Area
631 Monitoring and Assessment Program (SEAMAP) in the GoM. The cruise data are publicly
632 available on the NOAA National Centers for Environmental Information (NCOI) portal
633 (<https://www.ncei.noaa.gov/>), in the Oceans dataset. We thank L. Johns for useful suggestions
634 that improved the manuscript. We are grateful to G. Schmahl, E. Hickerson, S. Gittings, and G.
635 Sedberry of the NOAA National Marine Sanctuaries for their insightful comments in
636 discussions leading to this manuscript. We are grateful to S. DiMarco of Texas A&M
637 University for sharing observation data. We are grateful to the Flower Garden Banks National
638 Marine Sanctuary managers, in particular M. Johnston, for fruitful discussions and their interest
639 in the unique episode discussed herein, which led to organizing the 2016 Flower Garden Banks
640 Localized Mortality Event Mini-Symposium (Galveston, TX, February 27-28, 2018). We thank
641 two anonymous reviewers for their help in improving our manuscript.

642

643 **References**

644 - Altieri, A. H., S. B. Harrison, J. Seemann, R. Collin, R. J. Diaz, and N. Knowlton
645 (2017), Tropical dead zones and mass mortalities on coral reefs. *Proc. Natl. Acad. Sci. USA*,
646 114(14), pp.3660-3665.

647 - Androulidakis, Y.S., V.H. Kourafalou and R. Schiller (2015), Process studies on the
648 Mississippi River plume: impact of topography, wind and discharge conditions. *Cont. Shelf*
649 *Res.*, (107)33-49, doi:10.1016/j.csr.2015.07.014.

650 - Androulidakis, Y., V.H. Kourafalou, M. Le Hénaff, H.-S. Kang, T. Sutton, S. Chen, C.
651 Hu, N. Ntaganou (2019), Offshore spreading of Mississippi waters: pathways and vertical
652 structure under eddy influence, *J. Geophys. Res.*, 124, 5952–5978.

653 - Arnone, R., R. Vandermuelen, I. Soto, S. Ladner, M. Ondrusek, and H. Yang (2017),
654 Diurnal changes in ocean color sensed in satellite imagery. *J. App. Rem Sens.*, 11(3).

655 - Bianchi, T. S., S. F. DiMarco, J. H. Cowan, R. D. Hetland, P. Chapman, J. W. Day,
656 and M. A. Allison (2010), The science of hypoxia in the Northern Gulf of Mexico: a review.
657 *Science of the Total Environment*, 408(7), 1471-1484.

658 - Biggs, D. C., and F. E. Muller-Karger (1994), Ship and satellite observations of
659 chlorophyll stocks in warm- and cold-core rings in the western Gulf of Mexico. *J. Geophys.*
660 *Res.* (99:C4). 7,371-7,384.

661 - Bleck, R. (2002), An oceanic general circulation model framed in hybrid isopycnic-
662 Cartesian coordinates. *Ocean modelling*, 4(1), pp.55-88.

663 - Breaker, B. K., K. M. Watson, P. A. Ensminger, J. B. Storm, and C. E. Rose (2016),
664 Characterization of peak streamflows and flood inundation of selected areas in Louisiana,
665 Texas, Arkansas, and Mississippi from flood of March 2016: U.S. Geological Survey Scientific
666 Investigations Report 2016–5162, 33 p.

667 - Brown, C. A., Y. Huot, P. J. Werdell, B. Gentili, H. Claustre (2008), The origin and
668 global distribution of second order variability in satellite ocean color and its potential

669 applications to algorithm development. *Remote Sensing of Environment*. 112. 4186–4203.
670 doi:10.1016/j.rse.2008.06.008.

671 - Brown, A.L. and R.C. Carpenter (2013), Water-flow mediated oxygen dynamics
672 within massive Porites-algal turf interactions. *Mar. Ecol. Prog. Ser.*, 490, pp.1-10.

673 - Conley, D. J., H. W. Paerl, R. W. Howarth, D. F. Boesch, S. P. Seitzinger, E. Karl, E.
674 Karl, C. Lancelot, E. Gene, and E. Gene (2009), Controlling eutrophication: nitrogen and
675 phosphorus. *Science*, 123, pp.1014-1015.

676 - Dale, V., T. Bianchi, A. Blumberg, W., Boynton, D. J. Conley, W. Crumpton, M.
677 David, D. Gilbert, R. Howarth, C. Kling, and R. Lowrance (2007), Hypoxia in the northern
678 Gulf of Mexico: an update by the EPA Science Advisory Board. In EPA-SAB-08-003. EPA
679 Science Advisory Board Washington, DC.

680 - DiMarco, S. F. and R. O. Reid (1998), Characterization of the principal tidal current
681 constituents on the Texas-Louisiana shelf. *J. Geophys. Res.*, 103(C2), pp.3093-3109.

682 - DiMarco, S. F., J. Strauss, N. May, R. L. Mullins-Perry, E. L. Grossman, and D.
683 Shormann (2012), Texas coastal hypoxia linked to Brazos River discharge as revealed by
684 oxygen isotopes. *Aquat. Geochem.*, 18(2), pp.159-181.

685 - D'Sa, E., R. L. Miller, and B. A. McKee (2007), Suspended particulate matter
686 dynamics in coastal waters from ocean color: Application to the northern Gulf of Mexico.
687 *Geophys. Res. Lett.* 34 (L23611).

688 - Fournier, S., J. T. Reager, T. Lee, J. Vazquez-Cuervo, C. H. David, and M. M. Gierach
689 (2016), SMAP observes flooding from land to sea: The Texas event of 2015, *Geophys. Res.*
690 *Lett.*, 43, doi:10.1002/2016GL070821.

691 - Haas, A.F., J.E. Smith, M. Thompson, and D.D. Deheyn (2014), Effects of reduced
692 dissolved oxygen concentrations on physiology and fluorescence of hermatypic corals and
693 benthic algae. *PeerJ*, 2, p.e235.

694 - Hamilton, P., T. J. Berger, and W. Johnson (2002), On the structure and motions of
695 cyclones in the northern Gulf of Mexico. *J. Geophys. Res.*, 107(C12).

696 - Hetland, R. D. and S. F. DiMarco (2008), How does the character of oxygen demand
697 control the structure of hypoxia on the Texas–Louisiana continental shelf? *J. Marine Sys.*,
698 70(1), pp.49-62.

699 - Hickerson, E. L., G. P. Schmahl, M. Robbart, W. F. Precht, and C. Caldow (2008), The
700 state of coral reef ecosystems of the Flower Garden Banks, Stetson Bank, and other banks in
701 the northwestern Gulf of Mexico. The state of coral reef ecosystems of the United States and
702 Pacific Freely Associated States, pp.189-217.

703 - Hu, C., K. E. Hackett, M. K Callahan, S. Andréfouët, J. L. Wheaton, J. W. Porter, and
704 F. E. Muller-Karger (2003), The 2002 ocean color anomaly in the Florida Bight: A cause of
705 local coral reef decline? *Geophys. Res. Lett.*, 30(3).

706 - Hu., C., and F. Muller-Karger (2008), On the Connectivity and “Black Water”
707 Phenomena near the FKNMS: A Remote Sensing Perspective. In: Keller, B.D., and F.C.
708 Wilmot, eds. 2008. Connectivity: science, people and policy in the Florida Keys National
709 Marine Sanctuary. Colloquium proceedings, 19-21 August 2004, Key West, FL. Marine
710 Sanctuaries Conservation Series NMSP-08-02. U.S. Department of Commerce, National
711 Oceanic and Atmospheric Administration; National Marine Sanctuary Program, Silver Spring,
712 MD. p. 47.

713 - Hu, C., Z. Lee, and B. Franz (2012), Chlorophyll a algorithms for oligotrophic oceans:
714 A novel approach based on three-band reflectance difference. *J. Geophys. Res.*, 117(C1). doi:
715 10.1029/2011jc007395.

716 - Johnston, M. A, M. F. Nuttall, R. J. Eckert, R. D. Blakeway, T. K. Sterne, E. L.
717 Hickerson, G. P. Schmahl, M. T. Lee, J. MacMillan, and J. A. Embesi (2019), Localized coral
718 reef mortality event at East Flower Garden Bank, Gulf of Mexico, *Bull. Mar. Sci.*.

719 - Kourafalou V. H., T. N. Lee, L. Y. Oey, and J. D. Wang (1996), The fate of river
720 discharge on the continental shelf, 2: transport of coastal low salinity waters under realistic
721 wind and tidal forcing. *J. Geophys. Res.* 101(C2):3435–3455.

722 - Le Hénaff, M. and V.H. Kourafalou (2016), Mississippi waters reaching South Florida
723 reefs under no flood conditions: synthesis of observing and modeling system findings. *Ocean*
724 *Dynamics*, 66(3), pp.435-459.

725 - Lenihan, H.S., M. Adjeroud, M.J. Kotchen, J.L. Hench, and T. Nakamura (2008), Reef
726 structure regulates small-scale spatial variation in coral bleaching. *Mar. Ecol. Prog. Ser.*, 370,
727 pp.127-141.

728 - Levin, L. A., W. Ekau, A. J. Gooday, F. Jorissen, J. J. Middelburg, S. W. A. Naqvi, C.
729 Neira, N. N. Rabalais, and J. Zhang (2009), Effects of natural and human-induced hypoxia on
730 coastal benthos.

731 - Lowe, R.J. and J.L. Falter (2015), Oceanic forcing of coral reefs. *Annu. Rev. Mar. Sci.*,
732 7, pp.43-66.

733 - Morey S. L., P. J. Martin, J. J. O'Brien, A. A. Wallcraft, and J. Zavala-Hidalgo (2003),
734 Export pathways for river discharged fresh water in the northern Gulf of Mexico. *J. Geophys.*
735 *Res.* 108(C10):3303.

736 - Muller-Karger, F. E., J. J. Walsh, R. H. Evans, and M. B. Meyers (1991), On the
737 Seasonal Phytoplankton Concentration and Sea Surface Temperature Cycles of the Gulf of
738 Mexico as Determined by Satellites. *Journal of Geophysical Research.* 96(C7). 12645-12665.

739 - Muller-Karger, F. E. (2000), The Spring 1998 NEGOM Cold Water Event: Remote
740 Sensing Evidence for Upwelling and for Eastward Advection of Mississippi Water (or: How an
741 Errant LC Anticyclone Took the NEGOM for a Spin). *Gulf of Mexico Science.* 1. 55-67.

742 - Muller-Karger, Frank E., Joseph P. Smith, Sandra Werner, Robert Chen, Mitchell
743 Roffer, Yanyun Liu, Barbara Muhling, David Lindo-Atichati, John Lamkin, Sergio Cerdeira-
744 Estrada, and David B. Enfield (2015), Natural Variability of Surface Oceanographic Conditions
745 in the Offshore Gulf of Mexico. *Progress in Oceanography.* 10.1016/j.pocean.2014.12.007.

746 - Nababan, B., F. E. Muller-Karger, C. Hu, and D. C. Biggs (2011), Chlorophyll
747 variability in the northeastern Gulf of Mexico. *Int. J. Remote Sens.*, 32(23), pp.8373-8391.

748 - Nakamura, T. and R. Van Woesik (2001), Water-flow rates and passive diffusion
749 partially explain differential survival of corals during the 1998 bleaching event. *Mar. Ecol.*
750 *Prog. Ser.*, 212, pp.301-304.

751 - Nakamura, T., R. Van Woesik, and H. Yamasaki (2005), Photoinhibition of
752 photosynthesis is reduced by water flow in the reef-building coral *Acropora digitifera*. *Mar.*
753 *Ecol. Prog. Ser.*, 301, pp.109-118.

754 - Nepf, H.M. (2012), Flow and transport in regions with aquatic vegetation. *Annu. Rev.*
755 *Fluid Mech.*, 44, pp.123-142.

756 - Nepf, H.M., and E.R. Vivoni (2000), Flow structure in depth-limited, vegetated flow.
757 *J. Geophys. Res.*, 105(C12), pp.28547-28557.

758 - Nowlin, W. D., A. E. Jochens, S. F. DiMarco, R. O. Reid, and M. K. Howard (2005),
759 Low-frequency circulation over the Texas-Louisiana continental shelf. In : *Circulation in the*
760 *Gulf of Mexico: Observations and models*, eds. W. Sturges and A. Lugo-Fernandez, pp.219-
761 240, AGU, Washington, D. C.

762 - O'reilly, J.E. (2000), Ocean color chlorophyll a algorithms for SeaWiFS, OC2, and
763 OC4: Version 4. SeaWiFS postlaunch calibration and validation analyses, 3, pp.9-23.

764 - Otis, D. B. (2012), Spatial and Temporal Variability of Remotely Sensed Ocean Color
765 Parameters in Coral Reef Regions. Graduate Theses and Dissertations.
766 <https://scholarcommons.usf.edu/etd/4379>. Accessed 31 May 2019.

767 - Otis, D.B., M. Le Hénaff, V.H. Kourafalou, L. McEachron, L. and F.E. Muller-Karger
768 (2019), Mississippi River and Campeche Bank (Gulf of Mexico) Episodes of Cross-Shelf
769 Export of Coastal Waters Observed with Satellites. *Remote Sens.*, 11(6), p.723.

770 - Pomeroy, A.W., R.J. Lowe, M. Ghisalberti, C. Storlazzi, G. Symonds, and D. Roelvink
771 (2017), Sediment transport in the presence of large reef bottom roughness. *J. Geophys. Res.*
772 122(2), pp.1347-1368.

773 - Rabalais N. N., R. E. Turner, eds. (2001), *Coastal Hypoxia: Consequences for Living*
774 *Re- sources and Ecosystems*. American Geophysical Union. Washington, DC.

775 - Rabalais, N. N., R. E. Turner, and W. J. Wiseman Jr (2002), Gulf of Mexico hypoxia,
776 aka “The dead zone”. *Annual Review of ecology and Systematics*, 33(1), pp.235-263.

777 - Schaeffer, B. A., R. N. Conmy, A. E. Duffy, J. Aukamp, D. F. Yates, and G. Craven
778 (2015), Northern Gulf of Mexico estuarine coloured dissolved organic matter derived from
779 MODIS data. *Int. J. Rem. Sens.* 36(8): pp. 2219-2237.

780 - Schiller, R.V., and V.H. Kourafalou (2010), Modeling river plume dynamics with the
781 HYbrid Coordinate Ocean Model. *Ocean Modelling*, 33(1-2), pp.101-117.

782 - Schiller R. V., V. H. Kourafalou, P. Hogan, N. D. Walker (2011), The dynamics of the
783 Mississippi River plume: impact of topography, wind and offshore forcing on the fate of plume
784 waters. *J. Geophys. Res.* 116(C6), C06029.

785 - Schmahl, G. P., E. L. Hickerson, and W. F. Precht (2008), Biology and ecology of
786 coral reefs and coral communities in the Flower Garden Banks region, northwestern Gulf of
787 Mexico. *Coral Reefs of the USA*, pp.221-261.

788 - Soto, I., S. Andrefouet, C. Hu, F. E. Muller-Karger, C. C. Wall, J. Sheng, B. G. Hatcher
789 (2009), Physical connectivity in the Mesoamerican Barrier Reef System inferred from 9 years
790 of ocean color observations. *Coral Reefs*. DOI 10.1007/s00338-009-0465-0.

791 - Spalding, M., and G. Bunting, G (2004), A guide to the coral reefs of the Caribbean.
792 Univ of California Press.

793 - TABS (Texas Automated Buoy System Database) (2018), College Station, TX:
794 Geochemical and Environmental Research Group, Texas A&M University; c2018, 14 January,
795 2017. Available from: <http://tabs.gerg.tamu.edu/Tglo>. Accessed 5 June 2019.

796 - Teague, W. J., H. W. Wijesekera, E. Jarosz, D. B. Fribance, A. Lugo-Fernández, and
797 Z. R. Hallock (2013), Current and hydrographic conditions at the East Flower Garden Bank in
798 2011. *Cont. Shelf Res.*, 63, pp.43-58.

799 - Walker N. D., O. K. Huh, L. J. Rouse Jr, S. P. Murray (1996), Evolution and structure
800 of a coastal squirt off the Mississippi River delta: Northern Gulf of Mexico. *J. Geophys. Res.*
801 101(C9):20643–20655.

802 - White, M., I. Bashmachnikov, J. Arístegui, and A. Martins (2007), Physical processes
803 and seamount productivity. *Seamounts: ecology, fisheries and conservation*, pp.65-84.

804 - Zavala-Hidalgo, J., A. Gallegos-García, B. Martínez-López, S. L. Morey, and J. J.
805 O'Brien (2006), Seasonal upwelling on the western and southern shelves of the Gulf of Mexico.
806 *Ocean Dynam.*, 56(3), pp.333-338.

807 - Zavala-Hidalgo, J., R. Romero-Centeno, A. Mateos-Jasso, S. L. Morey, and B.
808 Martínez-López (2014), The response of the Gulf of Mexico to wind and heat flux forcing:
809 What has been learned in recent years? *Atmósfera*, 27(3), pp.317-334.

810 - Zhang, W., R. D. Hetland, S. F. DiMarco, and K. Fennel (2015), Processes controlling
811 mid-water column oxygen minima over the Texas-Louisiana shelf. *J. Geophys. Res.*, 120(4),
812 pp.2800-2812.